



Contents lists available at ScienceDirect

Journal of Sound and Vibration

journal homepage: www.elsevier.com/locate/jsvi



DAMAS with compression computational grid for acoustic source mapping



Wei Ma ^{a,*}, Xun Liu ^b

^a School of Aeronautics and Astronautics, Shanghai Jiao Tong University, Shanghai, PR China

^b Shanghai KeyGo Technology Company Limited, Shanghai, PR China

ARTICLE INFO

Article history:

Received 12 January 2017

Received in revised form 10 March 2017

Accepted 26 March 2017

Available online 31 March 2017

Handling editor: L.G. Tham

Keywords:

Microphone arrays

Beamforming

DAMAS

Acoustic

ABSTRACT

Nowadays phased microphone arrays have become a standard technique for acoustic source mapping. Compared with the conventional delay-and-sum beamforming method, deconvolution approaches such as DAMAS successfully improve the spatial resolution, however require high computational effort. Without optimizing DAMAS algorithm, recently DAMAS with wavelet compression computational grid (denoted by DAMAS-CG1) has reduced significantly computational run time of DAMAS in applications (Ma & Liu, *J. Sound Vib.*, 395, 2017), however DAMAS-CG1 has an inevitable deficiency that the occurrence probability of aliasing increases slightly for complicated sound source. This paper proposes a novel algorithm that DAMAS with computational grid compressed by discarding grid points with non-positive beamforming (denoted by DAMAS-CG2). Application simulations and an airfoil trailing edge noise experiment show that DAMAS-CG2 not only reduces significantly the computational run time but also retains the spatial resolution of DAMAS on original grid. Moreover DAMAS-CG2 overcomes the inevitable deficiency of DAMAS-CG1, and is simpler and more practical than DAMAS-CG1, although DAMAS-CG2 is usually less effective than DAMAS-CG1.

© 2017 Elsevier Ltd. All rights reserved.

1. Introduction

Nowadays phased microphone arrays have become a standard technique for acoustic source mapping [1]. The conventional delay-and-sum (DAS) beamforming algorithm constructs a dirty map of source distributions from array microphone output pressure signals [2]. Although conventional DAS beamforming is simple and robust, its main disadvantages include poor spatial resolution particularly at low frequencies [3] and appearance of ghost sources due to side-lobe effects [4,5].

Deconvolution approaches have been developed to overcome the disadvantages of beamforming, through reconstructing a clear map of source distributions from dirty map by iteratively deconvolution. Dougherty and Stoker [6] first applied the CLEAN algorithm [7], a classical deconvolution algorithm in many fields of imaging such as optical and radio astronomy, in acoustic array measurements. Sijtsma [8] extended CLEAN to CLEAN-SC for coherent sources. Brooks and Humphreys [9,10] proposed DAMAS algorithm for sound source localization, and extended it to three-dimensional acoustic imagine [11] and for coherent acoustic sources [12]. DAMAS achieved much better results than other deconvolution algorithms in typical aero-acoustic applications at that time, and makes researchers fully aware of the advantages and feasibility of deconvolution, and

* Corresponding author.

E-mail address: mawei@sjtu.edu.cn (W. Ma).

thus is considered as the breakthrough for deconvolution in aeroacoustic. Unfortunately, DAMAS requires a significant high computational effort (such as run time and computer memory) compared with conventional beamforming. With less computational run time of deconvolution, it is possible to reduce significantly the cost of measurements, and to enhance the ability of real-time display and online analysis. Reducing computational effort of deconvolution is thus a persistent pursuit in acoustic array measurements.

In order to reduce computational run time, Dougherty [13] introduced spectral procedure into DAMAS and obtained a more efficient deconvolution algorithm DAMAS2. Spectral procedure is applied under the assumption that PSF is shift-invariant, tantamount to assuming that the source field consists of plane waves. However this assumption is invalid in most aeroacoustic applications, especially when the distance between the observation plane and the microphone array is not large compared with the extension of the region of interest. A lot of effects of researches have been devoted to applying more efficient deconvolution algorithms, such as NNLS [14], FFT-NNLS [15], SCDAMAS [16], generalized inverse beamforming [17, 18], linear programming [19, 20], compressive sensing algorithm [21, 22, 23, 24], FISTA [25], and OMP-DAMAS [26]. However these deconvolution algorithms still require a relatively high computational effort compared with conventional beamforming due to the inevitable iterations used in the deconvolution algorithms. In addition, deconvolution algorithms introduce new problems by replacing continuous source distributions with misleading spots.

To obtain algorithms with more efficiency and better performances, many researchers have drawn the attention of deconvolution algorithms back to more advanced beamforming algorithms. Sarradj [27] presented orthogonal beamforming, a fast beamforming that has an improved spatial resolution, based on an eigenvalue decomposition of the cross spectral matrix. Huang et al. [28] successfully used robust adaptive beamforming in aeroacoustic measurements by systematically choosing a small Tikhonov factor that give stable results. Robust adaptive beamforming mainly improves the spatial resolution of the conventional beamforming with high efficiency nearly the same as the conventional beamforming. Dougherty [29] recently proposed a novel nonlinear beamforming algorithms named functional beamforming used the mathematics of functions of matrices. Functional beamforming could obtain dramatic dynamic range, improved spatial resolution, and identical speed compared with conventional beamforming. Even these advanced beamforming algorithms improve the spatial resolution relative to conventional beamforming, but is not as good as deconvolution algorithms especially DAMAS.

For reducing computational run time of deconvolution, one strategy is applying more efficient deconvolution algorithms such as Fourier-based algorithms (e.g. DAMAS2 [15], FFT-NNLS [16]). Spectral procedures are applied in these Fourier-based algorithms, under an assumption that PSF is shift-invariant, tantamount to assuming that the source field consists of plane waves. However this assumption is invalid in most aeroacoustic applications, especially when the distance between the observation plane and the microphone array is not large compared with the extension of the region of interest.

An alternative strategy to reduce the computational run time of deconvolution is using compression computational grid that only contains the significant grid points and does not contain the redundant grid points. This strategy is based on the fact that computational run time of deconvolution decreases with the decrease of the number of computational grid. In previous work [30], DAMAS with wavelet compression computational grid (denoted by DAMAS-CG1) has reduced significantly computational run time of DAMAS in applications, particularly when sound sources are just located in a small extent compared with scanning plane and a band of angular frequency needs to be calculated. However DAMAS-CG1 has an inevitable deficiency that the occurrence probability of aliasing increasing slightly for complicated sound source.

In order to not only reduce the computational run time of DAMAS but also overcome the deficiency of DAMAS-CG1, in this paper we propose a novel algorithm that DAMAS with computational grid compressed by a new method (denoted by DAMAS-CG2). The rest of this paper is organized as follows. Conventional beamforming and DAMAS are introduced in Section 2. The

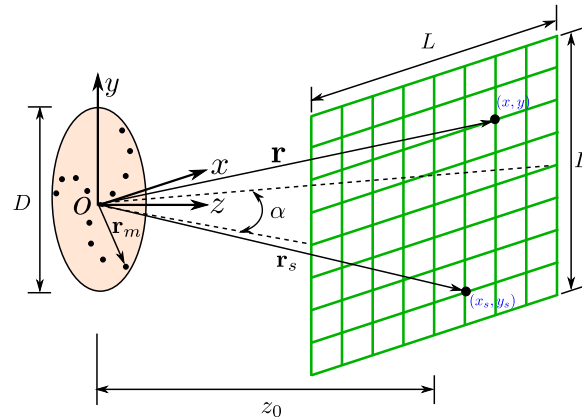


Fig. 1. Sketch of setup with a planar microphone array and a 2-D region of interest. Origin of the coordinate system is placed in the centre of the microphone array.

new algorithm DAMAS-CG2 is illustrated in [Section 3](#). Some application simulations are examined in [Section 4](#). An experimental application for aeroacoustic noise is examined in [Section 5](#). A discussion is presented in [Section 6](#). Finally, conclusions are given in [Section 7](#).

2. Conventional beamforming and DAMAS

[Fig. 1](#) illustrates a setup with a planar microphone array that contains M microphones and has a diameter of D , as well as a 2-D region of interest. Stationary noise sources are located in a x - y plane at a distance of z_0 from the centre of the microphone array. The length of the scanning plane is $L=2z_0\tan(\alpha/2)$, where α is the opening angle. The source plane is divided into $S=N\times N$ equidistant points.

In conventional beamforming, cross-spectral matrix (CSM) for each test case data set is firstly calculated using simultaneously acquired data from the microphone array. The acquired data of each microphone are divided into I frames. Each frame is then converted into frequency bins by Fast Fourier Transform (FFT). For a given angular frequency ω , CSM is averaged over I blocks

$$\mathbf{C}(\omega) = \overline{\mathbf{p}(\omega)\mathbf{p}(\omega)^H} = \frac{1}{I} \sum_{i=1}^I \mathbf{p}_i(\omega)\mathbf{p}_i(\omega)^H \quad (1)$$

where $\mathbf{p}(\omega) = [p_1(\omega), p_2(\omega), \dots, p_M(\omega)]^T$, $(\cdot)^H$ denotes complex conjugate transpose. For the sake of brevity, ω is omitted in the following. Notice that $\mathbf{C} \in \mathbb{C}^{M \times M}$. The conventional mean-square DAS beamforming output can then be written as

$$b(\mathbf{r}) = \frac{1}{M^2} \mathbf{e}(\mathbf{r})^H \mathbf{C} \mathbf{e}(\mathbf{r}) \quad (2)$$

where

$$\mathbf{e}(\mathbf{r}) = [e_1(\mathbf{r}), \dots, e_m(\mathbf{r}), \dots, e_M(\mathbf{r})]^T \quad (3)$$

is steering vector and $\mathbf{e}(\mathbf{r}) \in \mathbb{C}^{M \times 1}$, while the component for the m th microphone is

$$e_m(\mathbf{r}) = \frac{|\mathbf{r} - \mathbf{r}_m|}{|\mathbf{r}|} \exp\{-jk|\mathbf{r} - \mathbf{r}_m|\} \quad (4)$$

where $|\mathbf{r}|$ is the distance from the beamformer focus position to the centre of the array, $|\mathbf{r} - \mathbf{r}_m|$ is the distance from the beamformer focus position to the m th microphone (see in [Fig. 1](#)), and k is wavenumber and $k = \omega/c_0$, where c_0 is speed of sound.

The total sound pressure contribution at all microphones can be written as

$$\mathbf{p} = \mathbf{G}\mathbf{q} \quad (5)$$

where

$$\mathbf{G} = \begin{bmatrix} \bar{e}_1(\mathbf{r}_1) & \cdots & \bar{e}_1(\mathbf{r}_S) & \cdots & \bar{e}_1(\mathbf{r}_S) \\ \vdots & & \ddots & & \vdots \\ \bar{e}_m(\mathbf{r}_1) & \cdots & \bar{e}_m(\mathbf{r}_S) & \cdots & \bar{e}_m(\mathbf{r}_S) \\ \vdots & & \ddots & & \vdots \\ \bar{e}_M(\mathbf{r}_1) & \cdots & \bar{e}_M(\mathbf{r}_S) & \cdots & \bar{e}_M(\mathbf{r}_S) \end{bmatrix} \quad (6)$$

is a normalized propagation matrix whose element

$$\bar{e}_m(\mathbf{r}_S) = \frac{|\mathbf{r}_S|}{|\mathbf{r}_S - \mathbf{r}_m|} \exp\{-jk|\mathbf{r}_S - \mathbf{r}_m|\} \quad (7)$$

and

$$\mathbf{q} = [q_1, \dots, q_S, \dots, q_S]^T \quad (8)$$

is a vector of source amplitudes in terms of the pressure produced at the array centre. Notice that $\mathbf{p} \in \mathbb{C}^{M \times 1}$, $\mathbf{G} \in \mathbb{C}^{M \times S}$, $\mathbf{q} \in \mathbb{C}^{S \times 1}$. Submitting Eq. (5) to Eq. (1), and considering incoherent acoustic sources,

$$\mathbf{C} = \sum_{s=1}^S \overline{|q_s|^2} \cdot \bar{\mathbf{e}}(\mathbf{r}_s) \bar{\mathbf{e}}(\mathbf{r}_s)^H \quad (9)$$

where $\bar{\mathbf{e}}(\mathbf{r}_s)$ is column vector of \mathbf{G} (e.g. propagation vector),

$$\bar{\mathbf{e}}(\mathbf{r}_s) = [\bar{e}_1(\mathbf{r}_s), \dots, \bar{e}_m(\mathbf{r}_s), \dots, \bar{e}_M(\mathbf{r}_s)]^T \quad (10)$$

Notice that $\bar{\mathbf{e}}(\mathbf{r}_s) \in \mathbb{C}^{M \times 1}$. Eq. (2) can then be written as

$$b(\mathbf{r}) = \sum_{s=1}^S \overline{|q_s|^2} \cdot \frac{1}{M^2} \mathbf{e}(\mathbf{r})^H [\bar{\mathbf{e}}(\mathbf{r}_s) \bar{\mathbf{e}}(\mathbf{r}_s)^H] \mathbf{e}(\mathbf{r}) = \sum_{s=1}^S \overline{|q_s|^2} \cdot \frac{1}{M^2} |\mathbf{e}(\mathbf{r})^H \bar{\mathbf{e}}(\mathbf{r}_s)|^2 \quad (11)$$

For a single unit-power point source, Eq. (11) is known as point-spread function (PSF) of the array and is defined as

$$\text{PSF}(\mathbf{r}|\mathbf{r}_s) = \frac{1}{M^2} \mathbf{e}(\mathbf{r})^H [\bar{\mathbf{e}}(\mathbf{r}_s) \bar{\mathbf{e}}(\mathbf{r}_s)^H] \mathbf{e}(\mathbf{r}) = \frac{1}{M^2} |\mathbf{e}(\mathbf{r})^H \bar{\mathbf{e}}(\mathbf{r}_s)|^2 \quad (12)$$

and then Eq. (11) can then be written as

$$b(\mathbf{r}) = \sum_{s=1}^S \overline{|q_s|^2} \cdot \text{PSF}(\mathbf{r}|\mathbf{r}_s) \quad (13)$$

By computing $\text{PSF}(\mathbf{r}|\mathbf{r}_s)$ for all combinations of $(\mathbf{r}|\mathbf{r}_s)$ in discrete grid and arranging each resulting PSF map column-wise in a matrix \mathbf{A} , Eq. (13) could reformulate in matrix notation as

$$\mathbf{Ax} = \mathbf{b} \quad (14)$$

where \mathbf{b} contains the beamformer map, and $\mathbf{x} = [\overline{|q_1|^2}, \overline{|q_2|^2}, \dots, \overline{|q_S|^2}]^T$ is the source distribution of power descriptors. Eq. (14) is a system of linear equations. Notice that $\mathbf{A} \in \mathbb{C}^{S \times S}$, $\mathbf{x} \in \mathbb{C}^{S \times 1}$, $\mathbf{b} \in \mathbb{C}^{S \times 1}$. The deconvolution task is to find a source distribution \mathbf{x} for a given dirty map \mathbf{b} and a known matrix \mathbf{A} . The constraint is that each component of the vector \mathbf{x} is larger or equal to zero. In most of the applications the matrix \mathbf{A} is singular, and \mathbf{b} is in the range of \mathbf{A} , this means there are very large number of solutions of \mathbf{x} that fulfil Eq. (14).

The original DAMAS algorithm [10] is an iterative algebraic deconvolution method. In this algorithm, the source distribution is calculated by the solution of Eq. (14) using a Gauss-Seidel-type relaxation. In each step the constraint is applied that the source strength remains positive. The iteration step from solution $\mathbf{x}^{(n)}$ to $\mathbf{x}^{(n+1)}$ is given by the successive application of the scheme

$$r_i^{(n)} = \sum_{j=1}^{i-1} A_{ij} x_j^{(n+1)} + \sum_{j=i}^S A_{ij} x_j^{(n)} - b_i \quad (15)$$

and

$$x_i^{(n+1)} = \max \left(x_i^{(n)} - \frac{r_i^{(n)}}{A_{ii}}, 0 \right) \quad (16)$$

for $i=1, \dots, S$. The values A_{ij} , $x_j^{(n)}$ and b_i are components of the matrix \mathbf{A} and the vectors $\mathbf{x}^{(n)}$ and \mathbf{b} , respectively. Typically $\mathbf{x}^0 = \mathbf{0}$ is taken as initial solution. The value $r_i^{(n)}$ can be considered as the residual of the i th component in the step n .

The computation grid for DAMAS needs to be fine enough such that individual grid points along with other grid points represent a reasonable physical distribution of sources. In addition, too coarse grid may induce spatial aliasing from source distribution. In order to avoid aliasing problems, Brooks and Humphreys [10] recommended that $\Delta x/B \leq 0.2$, where Δx is spacing of grid points and B is array beamwidth of 3 dB down from beam peak maximum.

3. DAMAS-CG2

Diagonal removal (DR) is usually applied to CSM (Eq. (1)), by removing (zeroing out) the diagonal terms of CSM and accounting for this change in the number of terms of CMS in the denominator. This operation can remove the microphone self-

noise contamination particularly caused by turbulence interacting with the microphones, and thus improve dynamic range of the array results in poor signal-to-noise applications. Conventional beamforming (Eq. (2)) after DR comes to

$$b(\mathbf{r}) = \frac{\mathbf{e}(\mathbf{r})^H [\mathbf{C}]_{\text{diag}=0} \mathbf{e}(\mathbf{r})}{M^2 - M} \quad (17)$$

While DR is applied to CSM, conventional beamforming usually has negative values. These negative values are expected over low-level noise source regions in physical interpretation of resulting beamformer map. These grid points with non-positive beamforming could be considered as redundant points, and thus could be discarded from the original computation grid for scanning region. In this paper the computational grid is compressed by only reserving the grid points where

$$b(x, y) > \xi \quad (18)$$

and the threshold value

$$\xi = 0 \quad (19)$$

The original linear equations (Eq. (14)) on new irregular grid comes

$$\tilde{\mathbf{A}}\tilde{\mathbf{x}} = \tilde{\mathbf{b}} \quad (20)$$

where $\tilde{\mathbf{A}} \in \mathbb{C}^{\tilde{S} \times \tilde{S}}$, $\tilde{\mathbf{x}} \in \mathbb{C}^{\tilde{S} \times 1}$, $\tilde{\mathbf{b}} \in \mathbb{C}^{\tilde{S} \times 1}$, \tilde{S} is the number of compression computational grid points.

The algorithm, DAMAS with this new compression computational grid, is noted as DAMAS-CG2. [Algorithm 1](#) shows the processions of DAMAS-CG2. Step 1, conventional beamforming is calculated according to Eq. (17). Step 2, computational grid is compressed by only reserving the grid points with positive beamforming. Step 3, matrix $\tilde{\mathbf{b}}$ is obtained by reserving \mathbf{b} only on compression computational grid. Step 4, PSF is calculated according to Eq. (12) on compression computational grid. And then matrix $\tilde{\mathbf{A}}$ (e.g. \mathbf{A} on compression computational grid) is obtained by arranging each resulting PSF map column-wise in a matrix. Step 5, $\tilde{\mathbf{x}}$ is calculated from Eq. (20) using DAMAS algorithm. For run time of DAMAS with compression grid, the additional run times are (I) the time for grid compression in step 2 and (II) the calculation time of $\tilde{\mathbf{b}}$ in step 3, while the saved run times are mainly from (I) the calculation time of $\tilde{\mathbf{A}}$ in step 4 and (II) the iteration time in step 5 with less total number of grid points.

Algorithm 1. DAMAS-CG2

- 1: Calculate conventional beamforming according to Eq. (17);
- 2: Compress computational grid by reserving the grid points with positive beamforming (e.g. Eqs. (18) and (19));
- 3: Obtain matrix $\tilde{\mathbf{b}}$ by reserving \mathbf{b} only on compression computational grid;
- 4: Calculate PSF according to Eq. (12) on compression computational grid. And then arrange each resulting PSF map column-wise in a matrix $\tilde{\mathbf{A}}$ (e.g. \mathbf{A} on compression computational grid);
- 5: Calculate $\tilde{\mathbf{x}}$ from Eq. (20) using DAMAS algorithm.

4. Application simulations

In this section two application simulations are carried out on an Intel Core i5-2500K 3.30 GHz processor with MATLAB. The information of these two application simulations is listed in [Table 1](#). The planar array contains 30 microphones and has a diameter D of 0.35 m, as shown in [Fig. 2](#). In the geometrical setup, the observation plane is parallel to the array plane, and the region of interest is right in front of the array. The distance between array plane and observation plane z_0 is 0.5 m. The opening angle $\alpha=60^\circ$. In these simulations, the frequency f is 8 kHz. This corresponds to a wavelength of 0.043 m when the speed of sound c_0 is 340 m/s. The array beamwidth $B=1.22z_0c_0/(Df)$ is about 0.074 m. The original computational grid is 50×50 with 2500 grid points. The parameter $\Delta x/B$ is thus 0.16, falling in the range of [0.05, 0.2] recommended by Brooks and Humphreys [[10](#)]. Gaussian white noise is added with a signal-to-noise ratio of 15 dB at the microphone array. In each simulation, the source pressures q_s are assigned in the source distribution of power descriptors $\mathbf{x}=[\overline{|q_1|^2}, \overline{|q_2|^2}, \dots, \overline{|q_S|^2}]^T$. The corresponding beamformer map \mathbf{b} is then obtained according to Eq. (17). When applying DAMAS the deconvolution algorithm, the starting guess $\mathbf{x}^0=0$, and the number of iterations is 1000. The deconvolved maps already converge after 1000 iterations. Compression computational grid is obtained as introduced in previous section according to beamformer map. And then DAMAS is executed on compression grid.

Table 1

Information of application simulations.

Number of case	Case 1	Case 2
Arrray aperture diameter, D (m)	0.350	
Dis. between array plane and observation plane, z_0 (m)	0.5	
Opening angle, α	60°	
Scanning length, $L = 2z_0 \tan(\alpha/2)$ (m)	0.577	
Frequency, f (kHz)	8	
Array beamwidth, $B = 1.22z_0 c_0 / (Df)$ (m)	0.074	
Original grid	50×50	
Number of original grid points, S	2500	
$\Delta x/B$	0.16	
Number of iterations	1000	
Source power style	Two points	DAS image
Integrated source power set advance, $\sum \bar{x}$ (Pa ²)	1.000+0.100	42×1.000
Run time on original grid in step 4, T_4 (s)	301	301
Run time on original grid in step 5, T_5 (s)	93	93
Total run time on original grid, $T_{\text{DAMAS}} = T_4 + T_5$ (s)	394	394
Integrated source power on original grid, $\sum \bar{x}$ (Pa ²)	0.997+0.066	26.430
Error of integ. source power on ori. grid, $\eta = \frac{\sum \bar{x} - \sum x}{\sum \bar{x}}$	3.4%	37.0%
ξ	0	0
Number of compr. grid points, \tilde{S}	898	779
Compression ratio, $\sigma = S/\tilde{S}$	2.8	3.2
Run time on compression grid in step 2, T_2 (s)	0.04	0.04
Run time on compression grid in step 3, T_3 (s)	0.0001	0.0001
Run time on compression grid in step 4, T_4 (s)	39	29
Run time on compression grid in step 5, T_5 (s)	26	21
Total run time on compression grid, $T_{\text{DAMAS-CG2}} = T_2 + T_3 + T_4 + T_5 \approx T_4 + T_5$ (s)	65	50
Efficiency increasing, $\frac{T_{\text{DAMAS}} - T_{\text{DAMAS-CG2}}}{T_{\text{DAMAS}}}$	84%	87%
Integrated source power on compression grid, $\sum \tilde{x}$ (Pa ²)	0.997+0.066	26.430
Error of integ. source power on comp. grid, $\eta = \frac{\sum \tilde{x} - \sum \bar{x}}{\sum \bar{x}}$	3.4%	37.0%

4.1. Two points source with different source powers of 10 dB

In this simulation, synthetic two points source is placed at grid points (25, 25) and (31, 25). The source pressures q_s are defined to 1.000 Pa² at grid point (25, 25), 0.100 Pa² at grid point (31, 25), and 0 at all other grid points. The distance between these two source points is 0.07 m, smaller than the array beamwidth B . The level difference of the two sources is 10 dB. The corresponding beamformer map is shown in Fig. 3a. Only the larger source is clearly visible in the beamformer map. The deconvolved map after applying DAMAS algorithm to the beamformer map is shown in Fig. 3b. Two sources are well resolved by DAMAS on original grid with a very small error of source power of 3.2%. This small error of source power is due to noise signal added in the simulation.

The compression grid based on beamformer map is shown in Fig. 3c with blue circle points. The compression ratio is about 2.8. All the grid points with positive beamformer value are reserved in the compression grid, while grid points with zero and negative beamformer value are discarded as redundant points. Deconvolved map of DAMAS-CG2 is shown in Fig. 3d. The source positions are well resolved by DAMAS-CG2. The error of integrated source power on compression grid is as large as that on original grid. From the run time listed in Table 1, the run time of compression grid in step 2 is only 0.04 s, only half of the run time of DAMAS on original grid for 1 iteration, and thus is negligible compared with the total run time. The run time of calculating \mathbf{b} in step 3 is only 0.0001 s, and thus is also negligible compared with the total run time. The calculation takes

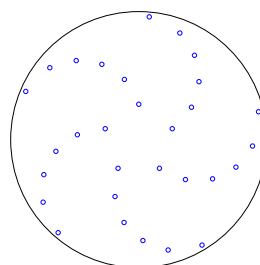


Fig. 2. Microphone array used in the experiment, with 30-channel irregular microphones and a diameter of 0.35 m.

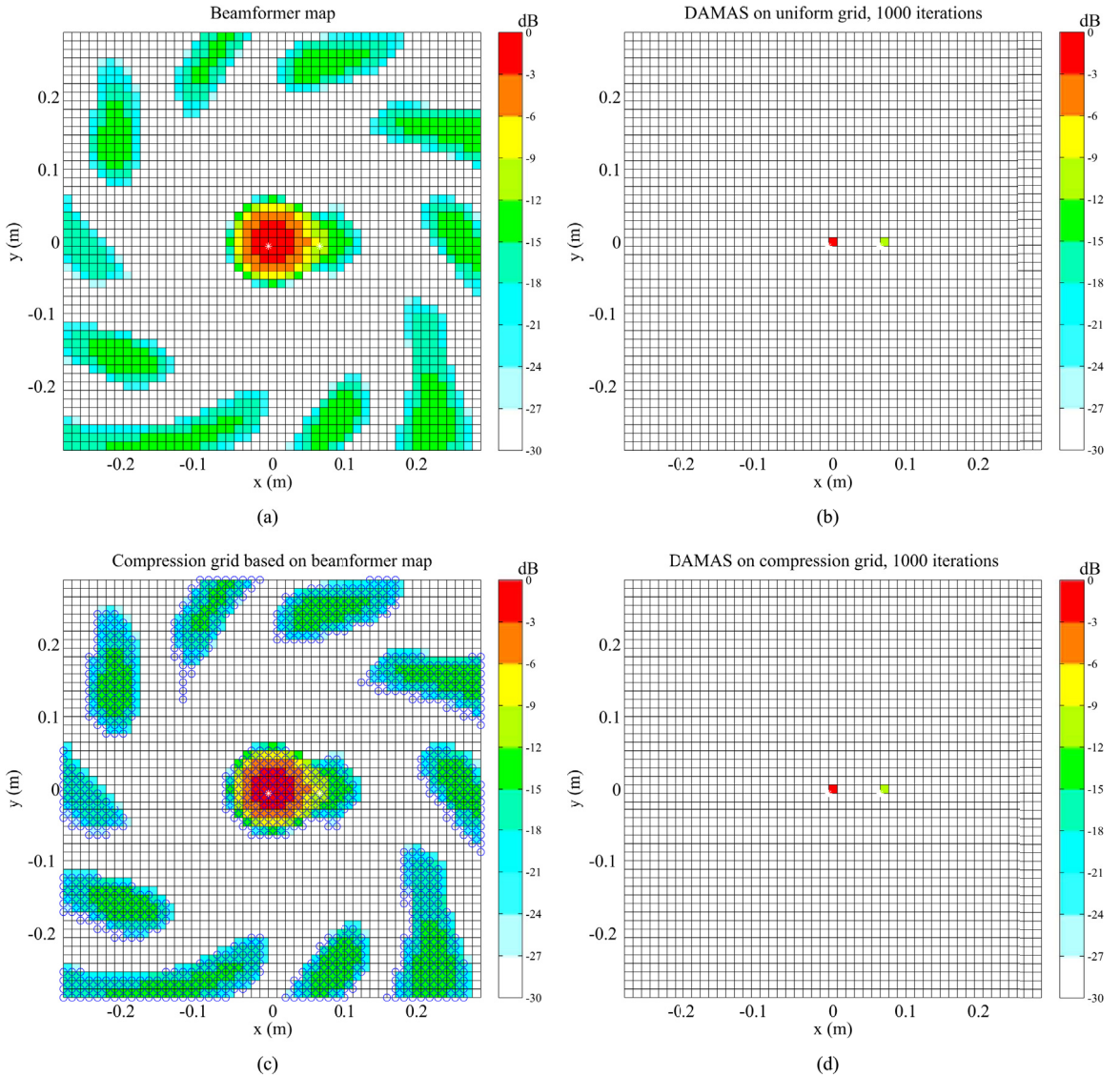


Fig. 3. Synthetic two points source, $f=8$ kHz. White cross symbols, positions of synthetic point sources. (a) Beamformer map. (b) Deconvolved map, DAMAS on original grid. (c) Compression grid based on beamformer map, shown by blue circles. (d) Deconvolved map, DAMAS-CG2. (For interpretation of the references to color in this figure legend, the reader is referred to the web version of this article.)

394 s on original grid while only about 65 s on compression grid. DAMAS-CG2 is thus about 84% faster than DAMAS on original computational grid.

This simulation verifies that DAMAS-CG2 reduces significantly the computational run time, while grid points with not positive beamformer value are discarded as redundant points in compression grid. Meanwhile spatial resolution of DAMAS-CG2 is the same as that of DAMAS on original grid in this simulation with two points simple source.

4.2. DAS image source

In this simulation, DAS image source as a complicated source is placed at grid points shown by the white cross symbols in Fig. 4a. The source pressures q_s are defined to 1.000 Pa^2 at these grid points and 0 at all other grid points. The corresponding beamformer map is shown in Fig. 4a. In this figure, the structure of source is very difficult to identify. The deconvolved map after applying DAMAS on the original grid is shown in Fig. 4b. The structure of source is identified to some degree. The error of integrated source power is about 37.0%. This error is mainly due to the deficiency of DAMAS for complicated sources, because the parameter $\Delta x/B$ is falling in the range recommended by Brooks and Humphreys [8] in order to avoid aliasing problems.

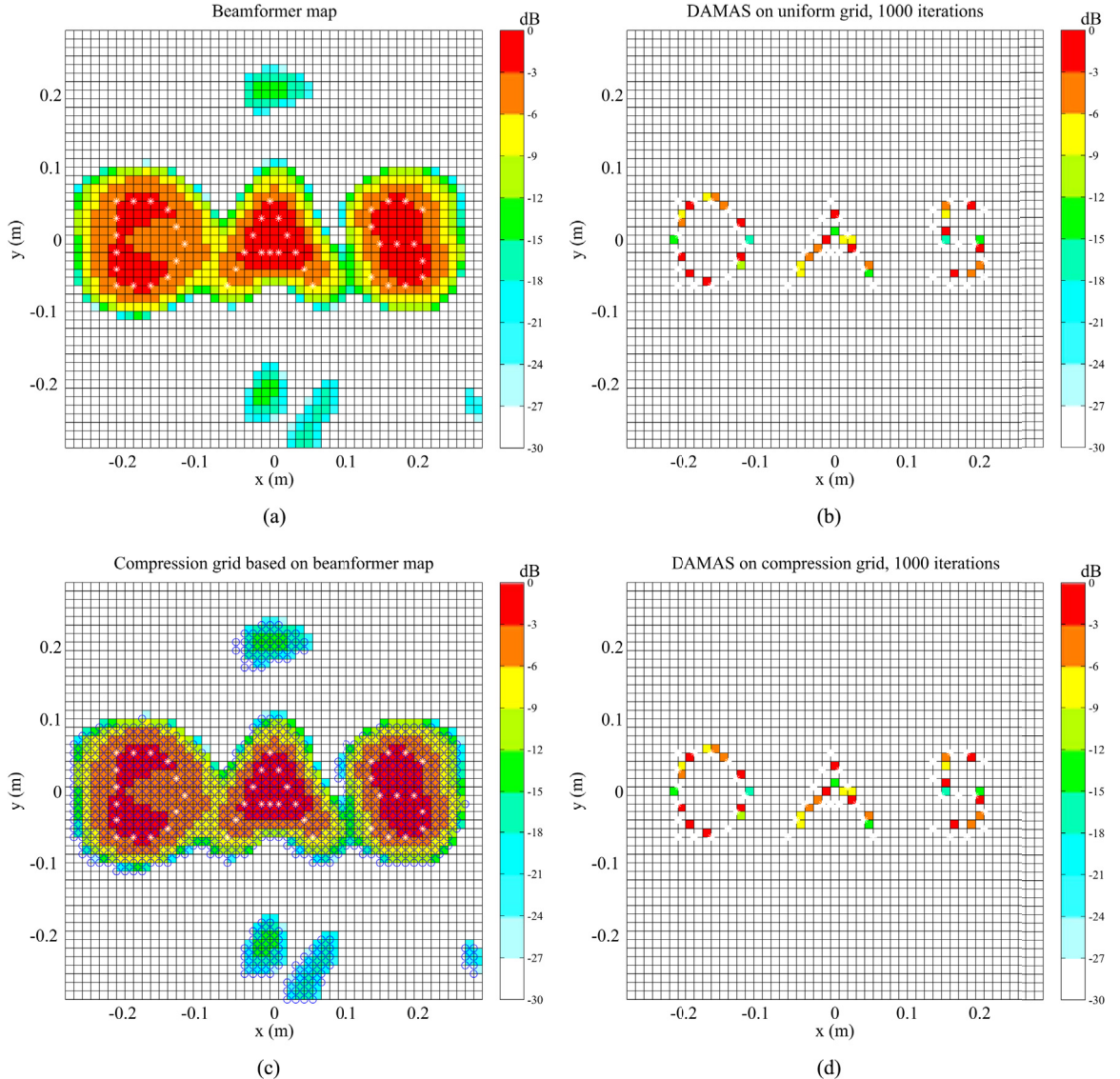


Fig. 4. Synthetic DAS image source, $f=8$ kHz. White cross symbols, positions of synthetic point sources. (a) Beamformer map. (b) Deconvolved map, DAMAS on original grid. (c) Compression grid based on beamformer map, shown by blue circles. (d) Deconvolved map, DAMAS-CG2. (For interpretation of the references to color in this figure legend, the reader is referred to the web version of this article.)

The compression grid based on beamformer map is shown in Fig. 4c with blue circle points. The compression ratio is about 3.2. The deconvolved map of DAMAS-CG2 is shown in Fig. 4d. In this figure, blue circles indicating compression grid don't appear for showing more clearly the structure of sound source. In Fig. 4d, the structure of source is substantially similar with that shown in Fig. 4b. The error of integrated source power of DAMAS-CG2 is equal to that of DAMAS on original grid. From the run time listed in Table 1, DAMAS on original grid takes 394 s while DAMAS-CG2 only takes about 50 s. DAMAS-CG2 is thus about 87% faster. As the previous case, the run times in step 2 and 3 are negligible compared with the total run time. DAMAS-CG2 reduces significantly the computational run time for this complex sound source.

4.3. Influence of SNR on DAMAS-CG2

Noise is inevitable in applications. In this section, influence of SNR on DAMAS-CG2 is investigated. In the former simulations, SNR is set as 15. In order to investigate the influence of SNR on DAMAS-CG2, both Case 1 and Case 2 with different SNR numbers are carried out.

For both DAMAS-CG2 and DAMAS on original grid, with the decreasing of SNR the accuracies of source locations and source powers of dirty maps consequentially decrease. As the simulations in the former two subsections, DAMAS-CG2 could

Table 2

Influence of SNR on DAMAS-CG2 in application simulations.

SNR	15	10	5
Case 1	Compression ratio	2.8 ± 0.05	
Case 2	Compression ratio	3.2 ± 0.05	

extract the same source distribution, including source locations and source powers, compared with DAMAS on original computational grid. And thus compression grid used in DAMAS-CG2 doesn't increase the influence of SNR on DAMAS in terms of source locations and source powers of dirty maps.

The developments of compression ratio of compression grid used in DAMAS-CG2 for Case 1 and Case 2 are listed in [Table 2](#). With decreasing SNR, compression ratios retain 2.8 and 3.2 for Case 1 and Case 2 respectively, with a very small fluctuation range (± 0.05) mainly due to the random number used to add noise in each simulation. This means that SNR doesn't influence too much on the compression ratio of the compression grid used in the DAMAS-CG2, and thus SNR doesn't influence too much the efficiency of DAMAS-CG2.

5. Experimental application

In this section, an airfoil trailing edge noise test is used to assess DAMAS-CG2. The data processing was carried out on the same computer as that used in application simulations. The experimental setup is shown in [Fig. 5](#). The information of this experimental application is listed in [Table 3](#).

A RAE2822 airfoil with 0.100 m chord is positioned at 0° angle-of-attack to the horizontal flow from the $0.18 \text{ m} \times 0.18 \text{ m}$ square nozzle of an open jet wind tunnel. The distance between the outlet of the nozzle and the airfoil leading edge is 0.300 m. The planar microphone array used in experiment is that used in [Section 4](#), which contains 30 microphones with irregular microphone positioning and has a diameter D of 0.35 m. The microphones are out-of-flow. And the distance between the microphone array plane and the airfoil (i.e. the observation plane) z_0 is 0.500 m. The opening angle $\alpha=40^\circ$. Microphone array data are acquired for 10 seconds with 25.6 kHz. Cross-spectral matrices are obtained by 0.1 s Hanning windows with 50% overlap to optimally smooth the spectra. In the experiment, the flow velocity at the nozzle outlet is 26.0 m/s, measured by a Pitot tube. The ambient temperature is 15° , and thus the speed of sound c_0 is 340 m/s. The experimental results are presented at the frequency f of 8.5 kHz. This corresponds to a wavelength of 0.040 m. The array beamwidth $B=1.22z_0c_0/(Df)$ is about 0.070 m. The original computational grid is 33×33 with 1089 grid points. The parameter $\Delta x/B$ is thus 0.16, satisfied the recommendation of Brooks and Humphreys [\[10\]](#) for avoiding aliasing problems. When applying DAMAS the deconvolution algorithm, the starting guess $x^0=0$, and the number of iterations is 1000.

The experimental beamformer map is shown in [Fig. 6a](#). Here the beamforming takes into account the modified propagation path due to shear layer refraction effects [\[31\]](#) with the simplified correlation described by Sijtsma [\[32\]](#). In this beamformer map, two noise regions along trailing edge are observed. The result after applying DAMAS algorithm on the original grid is shown in [Fig. 6b](#). Noise sources with better spatial resolution along trailing edge are well resolved by DAMAS on the original grid. The upper and lower points with higher sources are clearly visible. The compression grid based on beamformer map is shown in [Fig. 6c](#) with blue circle points. The tolerance $\xi=0$, and the compression ratio is about 2.8. The deconvolved map of DAMAS-CG2 is shown in [Fig. 6d](#). Noise sources with better spatial resolution along trailing edge are also well resolved by DAMAS-CG2. The locations of noise sources are nearly the same as that of DAMAS with the original grid in



Fig. 5. Experimental setup, an airfoil trailing edge noise.

Table 3

Information of experimental application.

Array aperture diameter, D (m)	0.35
Dis. between array plane and observation plane, z_0 (m)	0.5
Opening angle, α	40°
Scanning length, $L = 2z_0\tan(\alpha/2)$ (m)	0.364
Frequency, f (kHz)	8.5
Array beamwidth, $B=1.22z_0c_0/(Df)$ (m)	0.070
Original Grid	33×33
Number of original grid points, S	1089
$\Delta x/B$	0.16
Number of iterations	1000
Run time on original grid in step 4, T_4 (s)	60
Run time on original grid in step 5, T_5 (s)	29
Total run time on original grid, $T_{\text{DAMAS}}=T_4+T_5$ (s)	89
Integrated source power on original grid, $\sum x$ (Pa ²)	26.430
Number of compr. grid points, S'	391
Compression ratio, $\sigma = S/S'$	2.8
Run time on compression grid in step 2, T_2 (s)	0.0006
Run time on compression grid in step 3, T_3 (s)	0.0001
Run time on compression grid in step 4, T_4 (s)	7
Run time on compression grid in step 5, T_5 (s)	10
Total run time on compression grid, $T_{\text{DAMAS-CG2}}=T_2+T_3+T_4+T_5 \approx T_4+T_5$ (s)	17
Efficiency increasing, $\frac{T_{\text{DAMAS}} - T_{\text{DAMAS-CG2}}}{T_{\text{DAMAS}}}$	81%
Integrated source power on compression grid, $\sum \tilde{x}$ (Pa ²)	26.430

Fig. 6b. Meanwhile the differences of integrated source power of DAMAS on original grid and DAMAS-CG2 are the same. The run time of DAMAS on original grid and DAMAS-CG2 are about 89 and 17 seconds, respectively. And thus the efficiency of DAMAS at this experiment has been improved 81% through compression grid.

This experiment application clearly confirmed that for aeroacoustic noise DAMAS-CG2 could also improve significantly the efficiency of DAMAS and retain the reconstruction accuracy of DAMAS on original grid.

6. Discussion

In this paper in order to reduce computational run time of DAMAS for acoustic sound mapping, we propose a novel algorithm DAMAS-CG2, in which computational grid is compressed by discarding grid points with non-positive beamforming. This is mainly based on three foundational issues. The first issue is that computational run time of DAMAS decreases with the decrease of the number of computational grid. The second issue is that grid points with non-positive beamforming are redundant points in computational grid. The last issue is that DAMAS could extract the same source distribution on compression computational grid compared with that on original computational grid.

The main feature of DAMAS-CG2 is that DAMAS-CG2 uses compression grid by discarding grid points with non-positive beamforming. Except run time, DAMAS-CG2 reserves all the features of DAMAS with original computational grid, including spatial resolution, dynamic range, and accuracy of reconstruction source power. Concerning convergence speed, from the Gauss-Seidel-type relaxation (i.e. Eqs. (15) and (16)) used in DAMAS, DAMAS-CG2 has nearly the same convergence speed with DAMAS on original grid. As stated in Section 3 for run time of DAMAS-CG2, the additional run times are (I) the time for grid compression in step 2 and (II) the calculation time of $\tilde{\mathbf{b}}$ in step 3, while the saved run times are mainly from (I) the calculation time of $\tilde{\mathbf{A}}$ in step 4 and (II) the iteration time in step 5 with less total number of grid points. The additional run time is usually less than 0.1 s and thus is negligible compared with the saved run time. The computational run time reduction obtained with this method of course mainly depends on the compression ratio. The empirical formula between efficiency increasing ζ and compression ratio σ is that $\zeta \approx (1 - 1/\sigma^{1.7}) \times 100\%$, by statistics of many applications with various compression ratios. In applications that there are lots grid points with non-positive beamforming, compression ratio of compression grid will be much larger than one, and the computational run time of DAMAS could then be reduced significantly through compression computational grid. Concerning spatial resolution, DAMAS-CG2 retains the spatial resolution of DAMAS on original grid.

In DAMAS-CG1, computational grid is compressed by wavelet compression, and thus some grid points with positive beamforming are considered as redundant points. As a result compared with the DAMAS with original grid, the occurrence probability of aliasing increases particularly with larger threshold ϵ . Compared with DAMAS-CG1 (i.e. DAMAS with wavelet compression computational grid), DAMAS-CG2 is usually with smaller compression ratio, particularly when sound sources are located in a large extent compared with scanning plane. One example is the simulation that two points source with different source powers of 10 dB i.e. the Case 3 in [30] while the Case 1 in this paper. The compression ratio is 147 and 2.8 for DAMAS-CG1 and DAMAS-CG2, respectively. Consequentially DAMAS-CG2 is thus usually less efficient than DAMAS-CG1. However the occurrence probability of aliasing increasing does not increase in DAMAS-CG2, because computational grid of

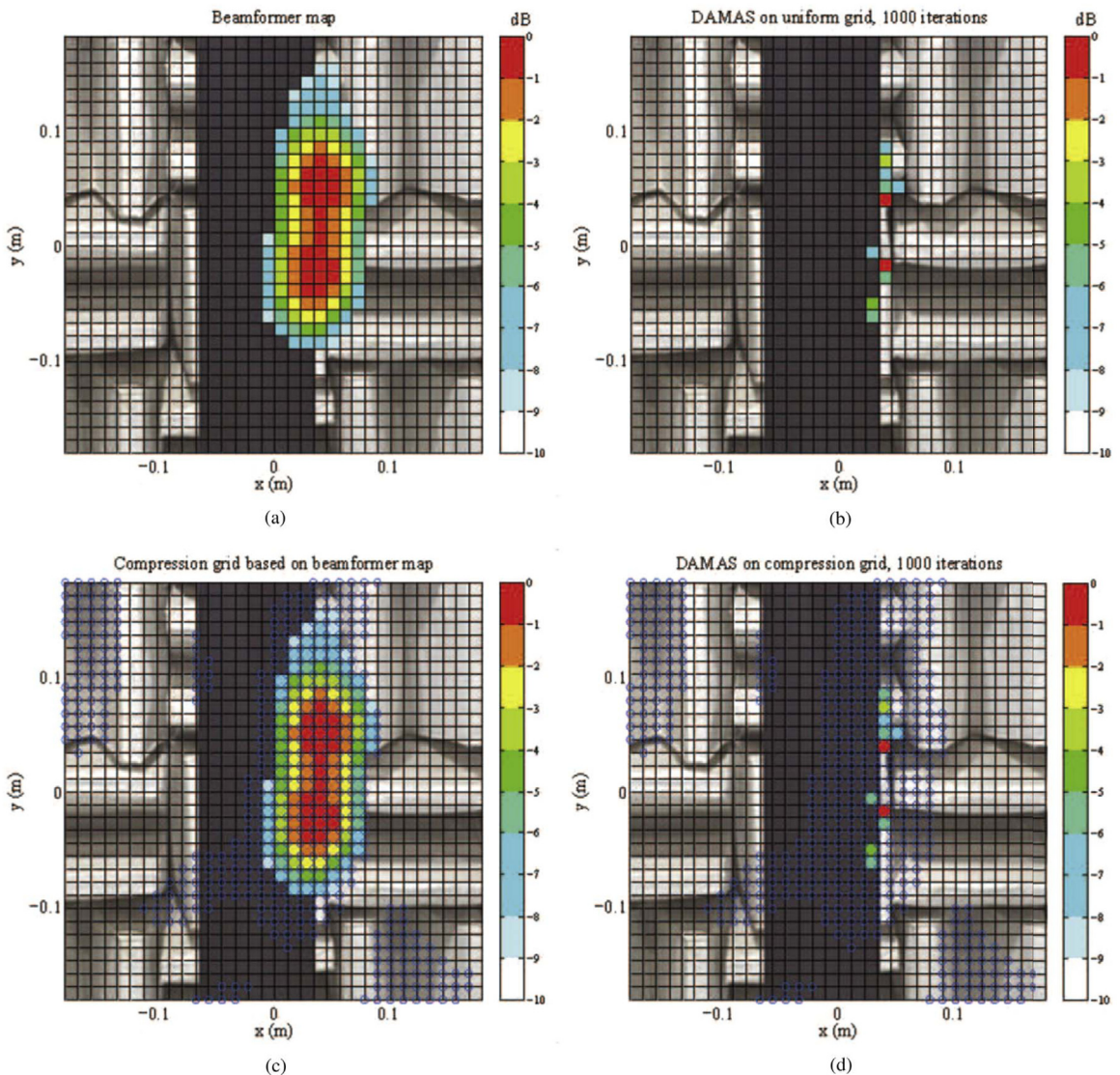


Fig. 6. Experiment, $f=8.5$ kHz. (a) Beamformer map. (b) Deconvolved map, DAMAS on original grid. (c) Compression grid based on beamformer map, shown by blue circles. (d) Deconvolved map, DAMAS-CG2. (For interpretation of the references to color in this figure legend, the reader is referred to the web version of this article.)

this new method contains all the grid points with positive beamforming. In addition, DAMAS-CG2 is simpler and more practical than DAMAS-CG1 from the comparison of these two algorithms.

In order to increase the compression ratio, the threshold value ξ in DAMAS-CG2, which is set as zero in this paper, could be set as the lower limit of the range that can be distinguished by DAMAS. In addition, the zero threshold value ξ is not appropriate any more in practical applications, particularly in low signal-to-noise ratio environments. The threshold value ξ can be adjusted to a proper larger value according to the signal-to-noise ratio in practical applications, in order to obtain a compression ratio as much as possible, and thus save computational run time as much as possible. This new larger threshold value ξ , of course, is usually different in each case, and thus could only be obtained only by seeking in each application. In some applications the plotting scale of dirty map has been determined in advance, and then a recommended value of ξ is the smallest beamforming value in the plotting scale.

As wavelet compression computational grid, the new method to compress the computational grid used in DAMAS-CG2 is also effective for DAMAS for three-dimensional acoustic imaging [11] which usually demands huge run time, and DAMAS-C [12] for coherent acoustic sources. Besides DAMAS, the new method to compress the computational grid used in DAMAS-CG2 could also be used to compress computational grid for other deconvolution algorithms introduced in Section 1 except those spectral-based algorithms.

7. Conclusion

This paper presents a novel and easy to use algorithm DAMAS-CG2 that DAMAS which computational grid compressed by discarding grid points with non-positive beamforming. In practical applications, this method could not only retain the spatial resolution of DAMAS on original grid, but also reduce lots of computational run time of DAMAS particularly when lots of computational grid with non-positive beamforming. Although DAMAS-CG2 is usually less effective than DAMAS-CG1 (i.e. DAMAS with wavelet computational grid), DAMAS-CG2 overcomes the inevitable deficiency of DAMAS-CG1 that the occurrence probability of aliasing increases slightly for complicated sound source. In addition, DAMAS-CG2 is simpler and more practical than DAMAS-CG1. For future investigations, it will be of interest to assess the efficiency of DAMAS-CG2 for moving sources as well as rotating sources.

Acknowledgement

The authors would like to thank three anonymous reviewers for their valuable comments. This work was supported by the Natural Science Foundation of Shanghai, China (Grant No. 15ZR1422500).

References

- [1] U. Michel, History of acoustic beamforming, in: Proceedings of the 1st Berlin Beamforming Conference, 2006, pp. 1–17.
- [2] D.H. Johnson, D.E. Dudgeon, Array Signal Processing: Concepts and Techniques, Prentice Hall, New Jersey, 1993.
- [3] J. Hald, J.J. Christensen, Technical Review: Beamforming, Brøel&Kjær, Danmark, 2004.
- [4] J. Hald, Array design optimized for both low-frequency NAH and high-frequency beamforming, in: Proceedings of the 33rd International Congress and Exposition on Noise Control Engineering, 2004, pp. 1–8.
- [5] A. Malgoezar, M. Snellen, P. Sijtsma, D. Simons, Improving beamforming by optimization of acoustic array microphone positions, in: Proceedings of the 6th Berlin Beamforming Conference, 2016, pp. 1–24. BeBeC-2016-S5.
- [6] R.P. Dougherty, R.W. Stoker, Sidelobe suppression for phased array aeroacoustic measurements, in: 4th AIAA/CEAS Aeroacoustics Conference, 1998.
- [7] J.A. Högbom, Aperture synthesis with a non-regular distribution of interferometer baselines, *Astronomy and Astrophysics Supplement Series* 15 (1974) 417–426.
- [8] P. Sijtsma, CLEAN based on spatial source coherence, *International Journal of Aeroacoustics* 6 (2007) 357–374.
- [9] T.F. Brooks, W.M. Humphreys, A deconvolution approach for the mapping of acoustic sources (DAMAS) determined from phased microphone arrays, AIAA-2004-2954 294 (2004) 856–879.
- [10] T.F. Brooks, W.M. Humphreys, A deconvolution approach for the mapping of acoustic sources (DAMAS) determined from phased microphone arrays, *Journal of Sound and Vibration* 294 (2006) 856–879.
- [11] T.F. Brooks, W.M. Humphreys, Three-dimensional application of DAMAS methodology for aeroacoustic noise source definition, AIAA 2005–2960 (2005).
- [12] T.F. Brooks, W.M. Humphreys, Extension of DAMAS phased array processing for spatial coherence determination (DAMAS-C), AIAA- 2006–2654 (2006).
- [13] R.P. Dougherty, Extension of DAMAS and benefits and limitations of deconvolution in beamforming, AIAA 2005–2961 (2005).
- [14] C.L. Lawson, R.J. Hanson, Solving Least Square Problems (Chapter 23), SIAM, 1995.
- [15] K. Ehrenfried, L. Koop, Comparison of iterative deconvolution algorithms for the mapping of acoustic sources, *AIAA Journal* 45 (2007) 1584–1595.
- [16] T. Yardibi, J. Li, P. Stoica, L.N. Cattafesta III, Sparsity constrained deconvolution approaches for acoustic source mapping, *Journal of the Acoustical Society of America* 123 (2008) 2631–2642.
- [17] T. Suzuki, L1 generalized inverse beam-forming algorithm resolving coherent/incoherent, distributed and multipole sources, *Journal of Sound and Vibration* 330 (2011) 5835–5851.
- [18] Z. Zhang, S. Chen, Z. Xu, Y. He, S. Li, Iterative regularization method in generalized invers beamforming, *Journal of Sound and Vibration* (2017).
- [19] R.P. Dougherty, R.C. Ramachandran, G. Raman, Deconvolution of sources in aeroacoustic images from phased microphone arrays using linear programming, *International Journal of Aeroacoustics* 12 (2013) 699–718.
- [20] N. Pignier, C.J. O'Reilly, S. Boij, Identifying equivalent sound sources from aeroacoustic simulations using a numerical phased array, *Journal of Sound and Vibration* 394 (2017) 203–219.
- [21] A. Xenaki, P. Gerstoft, K. Mosegaard, Compressive beamforming, *Journal of the Acoustical Society of America* 136 (2014) 260–271.
- [22] F. Ning, D. Gao, J. Niu, J. Wei, Combining compressive sensing with particle filter for tracking moving wideband sound sources, in: Signal Processing, Communications and Computing (ICSPCC), 2015 IEEE International Conference, 2015, pp. 1–6.
- [23] E. Fernández-Grande, A. Xenaki, Compressive sensing with a spherical microphone array, *Journal of the Acoustical Society of America* 139 (2016) EL45–EL49.
- [24] F. Ning, J. Wei, L. Qiu, H. Shi, X. Li, Three-dimensional acoustic imaging with planar microphone arrays and compressive sensing, *Journal of Sound and Vibration* 380 (2016) 112–128.
- [25] O. Lylloff, E. Fernández-Grande, F. Agerkvist, J. Hald, E.T. Roig, M.S. Andersen, Improving the efficiency of deconvolution algorithms for sound source localization, *Journal of the Acoustical Society of America* 138 (2015) 172–180.
- [26] T. Padois, A. Berry, Orthogonal matching pursuit applied to the deconvolution approach for the mapping of acoustic sources inverse problem, *Journal of the Acoustical Society of America* (2015).
- [27] E. Sarradj, A fast signal subspace approach for the determination of absolute levels from phased microphone array measurements, *Journal of Sound and Vibration* (2010).
- [28] X. Huang, I. Bai Long, Vinogradov, E. Peers, Adaptive beamforming for array signal processing in aeroacoustic measurements, *Journal of the Acoustical Society of America* 131 (2012) 2152–2161.
- [29] R.P. Dougherty, Functional beamforming, in: 5th Berlin Beamforming Conference 2014, 2014. BeBeC-2014–01.
- [30] W. Ma, X. Liu, Improving the efficiency of DAMAS for sound source localization via wavelet compression computational grid, *Journal of Sound and Vibration* 395 (2017) 341–353.
- [31] R. Amiet, Refraction of sound by a shear layer, *Journal of Sound and Vibration* 58 (1978).
- [32] P. Sijtsma, Phased array beamforming applied to wind tunnel and fly-over tests, NLR-TP-2010–549 (2010).